Sensors & Actuators: B. Chemical 390 (2023) 133937

Contents lists available at ScienceDirect

Sensors and Actuators: B. Chemical

journal homepage: www.elsevier.com/locate/snb

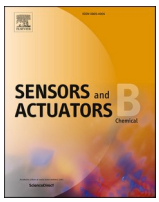

Ppb-level mid-IR quartz-enhanced photoacoustic sensor for sarin simulant detection using a T-shaped tuning fork

Zhijin Shang [a,b,1], Hongpeng Wu [a,b,1], Shangzhi Li [a,b], Gang Wang [a,b], Angelo Sampaolo [c], Pietro Patimisco [c], Vincenzo Spagnolo [a,c], Lei Dong [a,b,*]

[a] State Key Laboratory of Quantum Optics and Quantum Optics Devices, Institute of Laser Spectroscopy, Shanxi University, Taiyuan 030006, PR China
[b] Collaborative Innovation Center of Extreme Optics, Shanxi University, Taiyuan 030006, PR China
[c] PolySense Lab-Dipartimento Interateneo di Fisica, University and Politecnico of Bari, Via Amendola 173, Bari, Italy

ARTICLE INFO

Keywords:
Chemical warfare agent
Photoacoustic spectroscopy
Quartz tuning fork
Trace gas sensor

ABSTRACT

A ppb-level mid-IR quartz-enhanced photoacoustic sensor for the highly sensitive detection of dimethyl methyl phosphonate (DMMP) —the sarin simulant—is developed using a T-shaped tuning fork. The sensor employs a narrow-linewidth mid-IR quantum cascade laser (QCL) to target a strong, interference-free DMMP absorption band. A custom quartz tuning fork with 800-μm prong spacing is employed to avoid significant photothermal noise, thus removing the requirement for an optical spatial filter. The performance of the photoacoustic sensor was optimized in terms of exciting power, modulation frequency, and gas pressure. A minimum detection limit of 6 ppb was achieved at an integration time of 300 ms, which can be further improved to 0.45 ppb at the optimal integration time of 20 s

1. Introduction

The threat of chemical warfare agents (CWA), especially the highly lethal nerve agent represented by sarin (GB), is of great concern worldwide. The acute toxicity of the sarin nerve agent is due to its ability to quickly paralyze the central nervous system in small doses by combining it with acetylcholinesterase (AChE) in the neuromuscular junction of the central nervous system [1]. More worrisomely, due to the low cost and uncomplicated technology required for production, sarin has become the first choice for terrorists, which is not only a threat to soldiers on the battlefield but also to civilians in public places. For example, sarin was released by the Aum Shinrikyo sect in the crowded Tokyo subway in 1995, resulting in the hospitalization of 5,000 victims [2]. The highly sensitive nerve agent sensor capable of in situ monitoring has become an important research topic in response to the need for efficient and accurate detection of sarin agents in wars and terrorist attacks.

Because some organophosphorus compounds have similar chemical structures to sarin but are non-toxic, they are appropriate substitutes for operating the sarin nerve agent in a laboratory environment. Dimethyl methyl phosphonate (DMMP) is widely regarded as the most convincing sarin simulant [3–11]. Various gas analysis techniques have been developed and are widely used for sarin and DMMP detection. Gas chromatography (GC) and mass spectrometry (MS) analysis can identify the different organophosphorus compounds with high sensitivity, but they have several disadvantages for in situ monitoring, including being expensive and time-consuming [7]. Moreover, the chromatographic analysis must be performed in a specialized laboratory by skilled personnel and is not suitable for miniaturization. Miroslav et al. developed a colorimetric dipstick for the semi-quantitative assay of sarin and DMMP based on the discoloration reaction of pH papers [8]. The presence of sarin or DMMP would inhibit the enzymatic reaction on the dipstick, which was characterized by pH papers not responding. These colorimetric dipsticks have the advantage of being easy to prepare and small in size, but they suffer from poor sensitivity, insufficient selectivity, and susceptibility to changes in temperature and humidity. Surface acoustic wave (SAW) sensors have been demonstrated to achieve high sensitivity and selectivity by changing the chemo-selective polymers on the surface of the sensitive film [9]. SAW sensors can be small and portable but are sensitive to moisture and may suffer from

* Corresponding author at: State Key Laboratory of Quantum Optics and Quantum Optics Devices, Institute of Laser Spectroscopy, Shanxi University, Taiyuan 030006, PR China.
E-mail address: donglei@sxu.edu.cn (L. Dong).
[1] These authors contributed equally to this paper.

https://doi.org/10.1016/j.snb.2023.133937
Received 13 March 2023; Received in revised form 25 April 2023; Accepted 3 May 2023
Available online 5 May 2023

de-wetting effects that reduce responsiveness. The advantage of electrochemical sensors based on various semiconductor metal oxides lies in their ease of preparation and low cost. However, they are susceptible to environmental impurities that can produce false positives.

Compared with the above techniques, photoacoustic spectroscopy (PAS) is one of the most promising techniques for sarin gas level monitoring in public places due to its benefits of high sensitivity, selectivity, and fast response [12–17]. The quartz-enhanced photoacoustic spectroscopy (QEPAS) technique as a variant of PAS has rapidly developed since it was first reported in 2002, in which an ultra-narrowband quartz tuning fork (QTF) acoustically couples with two acoustic micro-resonators (AmRs) acting as a sharply resonant acoustic transducer to detect sound signals instead of conventional broadband microphones [18–41]. Compared with the sizes of the conventional photoacoustic cell, which is more than 10 cm^3, the small volume of QTF is more conducive to the miniaturization and rapid response of sarin or DMMP detection equipment. Besides, the remarkable feature of the QEPAS technique is the excitation wavelength independence, meaning that trace gases with different characteristic absorption spectra can be measured using the same spectrophone. Sarin and DMMP show strong optical absorption features in the mid-infrared region of 9–11.5 μm, so high detection sensitivity can be theoretically achieved using high-performance mid-infrared quantum cascade lasers (QCLs). However, the mid-infrared QCL output beam usually has a large divergence angle, which makes it a great challenge to couple a mid-infrared laser beam through a 300-μm prong-spacing QTF since any stray light hitting the QTF can cause a large background signal.

In this work, we demonstrate a miniaturized and integrated QEPAS-based DMMP sensor, in which a custom T-shaped QTF and a mid-infrared quantum cascade laser (QCL) are used. The T-shaped QTF has a prong spacing of 0.8 mm and a high-quality factor of ~ 15,000, avoiding the background signal caused by stray light, thus obtaining an optimal detection limit at the ppb level. The DMMP sensor was tested using real outdoor air mixed with DMMP to verify its effectiveness.

2. Experimental section

2.1. Selection of detection wavelength and optical excitation source

A strong targeted absorption band is vital for DMMP detection because the practical application necessitates sensing devices with sub-parts-per-million sensitivities. The absorption spectra of the DMMP molecules between 7 μm and 16 μm were experimentally recorded by a Fourier transform infrared spectroscopy (FTIR) spectrometer (Thermofisher Nicolet IS50) equipped with a 9.5-m multipass gas cell. 1 ppm DMMP/N_2 mixture (Dalian special Gases Co., LTD, China) was filled into the gas cell at atmospheric pressure. The DMMP molecules show the strongest absorption characteristics in the vibration band centered at 1050 cm^{-1}, as shown by the solid red line in Fig. 1. Potential spectral interference comes from H_2O and CO_2, which are important components of air. According to the HITRAN database, there is no spectral overlap between H_2O and CO_2 absorption lines, and the strongest absorption band of DMMP in such a wavelength region, as shown in Fig. 1. Therefore, the absorption band centered at 1050 cm^{-1} was determined to use as the target detection band.

QCLs have established their presence as the most versatile semiconductor excitation source in the mid-IR spectral region due to their high output power, compactness, and narrow spectral linewidth. Considering the excitation wavelength and size of the laser source, a QCL laser (Ningbo Healthy Photo Technology, QC-Qube 200831-AC712) with an emission wavelength of 9.5 μm and a linewidth of 2 MHz was employed as the excitation source of the DMMP-QEPAS sensor, which has an output power stability of < 2 %. The QCL laser driving circuit (Healthy Photon QC750-Touch™) with extremely low current noise and temperature drift operated at room temperature for stabilizing the emitting wavelength. The temperature of the QCL was set

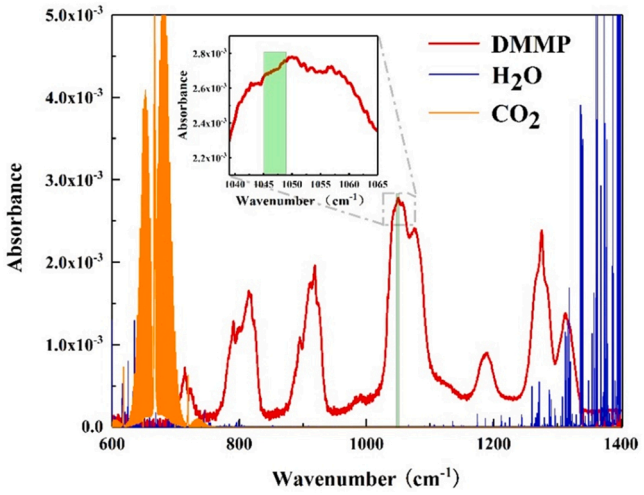

Fig. 1. Absorption spectra of 1-ppm DMMP/N_2 gas mixture (red) obtained by the FTIR spectrometer and absorption spectra of 300-ppm H_2O (blue) and 5-ppm CO_2 (orange) based on HITRAN database. Inset: DMMP absorption band in the range of 1040–1065 cm^{-1} and wavelength tuning range of the used QCL laser.

to 25.5 ℃ by means of the laser driving circuit. As shown in Fig. 2, the output wavelength of the QCL laser used is a function of the driving current and its wavelength tuning range fall in the selected absorption band (the green box area in Fig. 1). In QEPAS sensing, the amplitude modulation technique is required for the detection of molecules with unsolved broadband absorption features, resulting in half the average output optical power of the unmodulated mode. The linear relationship between the average power of the QCL laser and the driving current was plotted in Fig. 2, demonstrating good linearity. Moreover, the small size is a noticeable feature of this laser source, which has an outside dimension of ~ 300 cm^3 (65 × 65 × 70 mm^3), allowing the laser source to realize compact gas sensors.

2.2. Integrated QEPAS-based DMMP sensor design

The experimental setup for DMMP detection is sketched in Fig. 3(a), which includes an optical sensing system, an electrical control and data processing system, and a gas sampling system. In the optical part, the collimated light beam from the QCL was focused into a 0.4-mm-

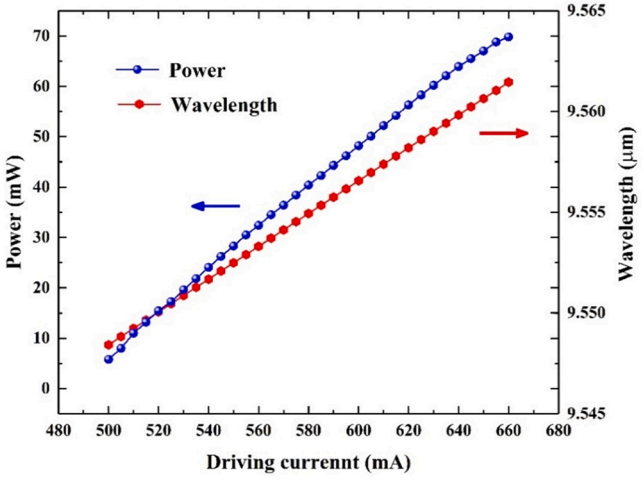

Fig. 2. QCL emission wavelength and output optical power as a function of driving current in amplitude modulation operating mode with a duty cycle of 50 %.

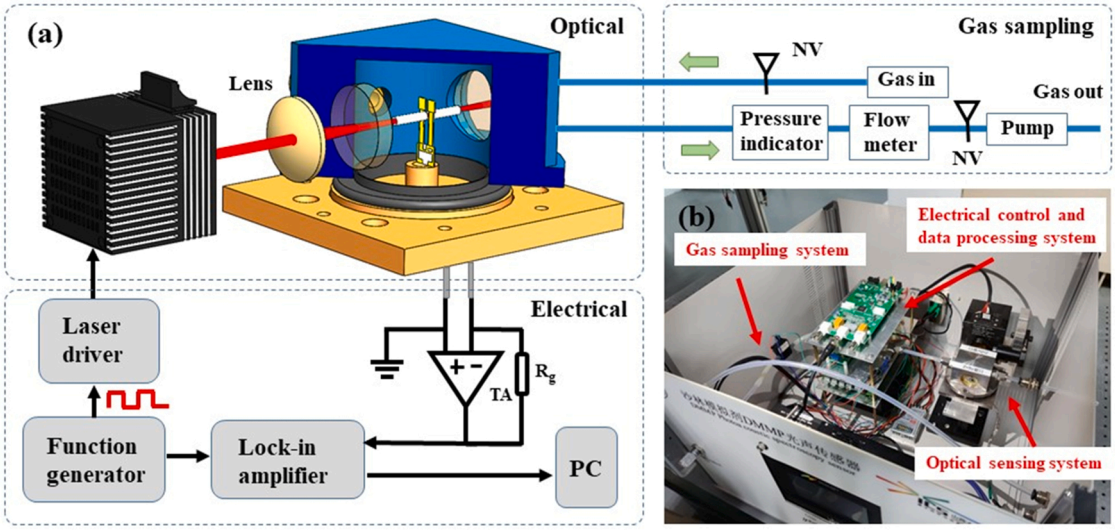

Fig. 3. (a) Schematic of the QEPAS-based DMMP sensor system. (b) Photograph of the QEPAS-based DMMP sensor with dimensions of length (35 cm), width (35 cm), and height (20 cm).

diameter light spot by the zinc selenide focusing lens with a focal length of 75 mm. Then the laser beam passed through a 70-cm^3 inner volume of the acoustic detection module (ADM), which consists of a spectrophone and a gas enclosure. Two zinc selenide (ZnSe) windows with diameters of 25.4 mm were mounted on either side of the gas enclosure for optical access. The ZnSe windows have a high transmissivity efficiency (95 %) at 9.5 μm. The QEPAS spectrophone was composed of a T-shaped QTF with a resonance frequency f_0 of 12.4 kHz and AmRs, which was installed at the focal point of the focusing lens to probe the acoustic energy accumulated inside the tube. Two identical AmRs with an inner diameter of 1.75 mm and an individual length of 13 mm were placed on both sides of the QTF and aligned vertically to the tuning fork facet, forming an on-beam QEPAS configuration. The resonator center was positioned 2 mm far from the QTF prongs top. A signal enhancement factor of ~ 30 was achieved with such an optimum configuration compared to the bare T-shaped QTF without AmRs.

The prong width of the T-shaped QTF is not a constant along the prong axis. The width function $T(x)$ of prongs is considered a piecewise function that can be written as:

$$T(x) = \begin{cases} T_1 & x\epsilon[0, L_0] \\ T_2 & x\epsilon[L_0, L_1] \end{cases} \quad (1)$$

The T-shaped QTF has dimensions of $T_1 = 2.0$ mm, $T_2 = 1.4$ mm, $L_0 = 2.4$ mm, $L_1 = 9.4$ mm, and has a prong spacing of 800 μm. The T-shaped QTF has an R-value of 104.35 kΩ and a Q-factor of 15,142. The increase in the top weight of the QTF can enhance the stress field of the prongs, increasing the piezoelectrically induced charges. As a result of this, the QTF current signal was improved.

In the electrical control and data processing system, a commercial waveform generator circuit board (Juntek MHS5200A) generated a square wave signal at the QTF resonance frequency (f =12 457 Hz) to drive the QCL current. The piezoelectric signal generated by the QTF was amplified by a homemade trans-impedance preamplifier with a feedback resistance of 10 MΩ and then sent to a lock-in amplifier board (FEMTO Inc., Germany, Model LIA-BVD-150-H) operating in 1 f mode. The time constant of the lock-in amplifier was set to 300 ms with a filter slope = 12 dB/oct, leading to a 0.833 Hz detection bandwidth. A laptop equipped with a 16-bit data acquisition card (DAQvantech, USB_HRF4626) was used to collect the data at a sampling rate of 250 kS/s. A Labview program was programmed to control all the data acquisition and processing.

The gas sampling system was designed to collect the gas in the environment and to regulate the gas pressure and flow, providing a suitable measurement environment for photoacoustic detection. Two needle valves and a vacuum pump (KNF Technology Co., Ltd., N816.3KT.18) were used to control the flow and pressure of the mixed gas in the ADM. A compact mass flow meter and a pressure indicator were installed downstream to monitor the gas flow rate and pressure inside the sensor system. The gas flow rate was set at a constant value of 270 standard cubic centimeters per minute (sccm) in all measurements to avoid the flow noise. To miniaturize the QEPAS-based sensor, we packaged system components into waterproof cases with external dimensions of 35 × 35 × 20 cm^3, and the prototype photo of the QEPAS-based DMMP sensor is shown in Fig. 3(b).

2.3. Optimization of the sensor performance

The unique advantage of QEPAS technology is that the sensitivity of QEPAS-based sensors is proportional to the actual optical power; thereby, the excitation power was optimized experimentally to improve the performance of the DMMP sensor. In this work, a certified 500 ppbv DMMP/zero air mixture was flushed into the ADM at room temperature of 25 ℃. The composition of zero air consists of ~ 79 % nitrogen and 21 % oxygen. In amplitude modulation mode, the measured signal and background noise were plotted as a function of the actual output optical power ranging from 5 mW to 70 mW, as shown in Fig. 4(a). The background noise levels were defined as the signal offset at different powers in zero air. A linear fitting procedure was performed to verify the relationship between optical power and signal amplitude. The calculated R-square of 0.997 confirmed that our sensor system did not operate in saturation. However, the amplitude modulation technique provides a strong fundamental wave component, resulting in serious coherent background noise caused by the high-power beam passing through the window. The signal-to-noise ratios (SNRs), as a more accurate parameter to evaluate sensor performance, were calculated and plotted in Fig. 4(b) according to the following equations:

$$\mathrm{SNR} = \frac{S_{QEPAS} - S_{BN}}{1\sigma} \quad (2)$$

where, S_{QEPAS}, S_{BN}, and 1σ are the QEPAS signal amplitude, the background noise, and the standard deviation of the signal, respectively. The SNR value increases gradually with the laser power increasing until a maximum is reached and then decreases. The maximum QEPAS SNR of 110 was achieved at laser power of 65.5 mW. Therefore, further

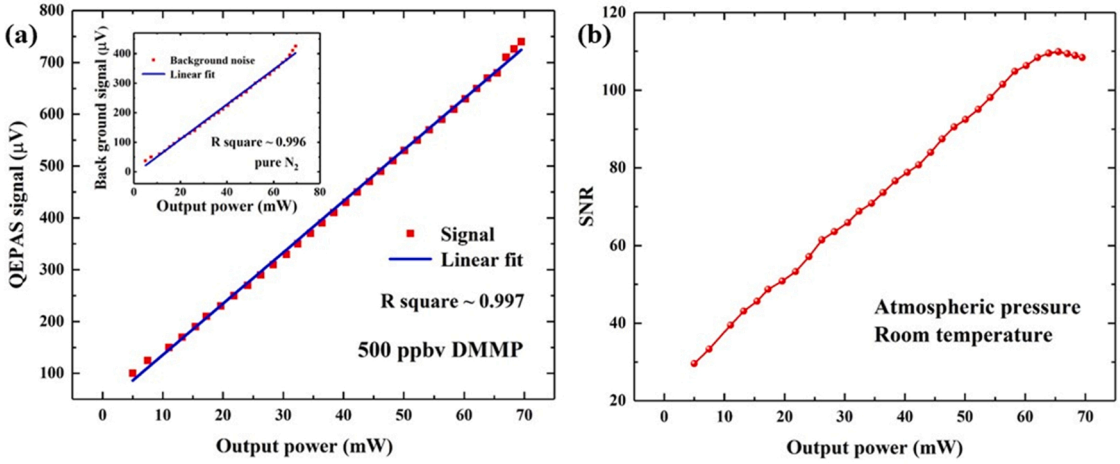

Fig. 4. (a) QEPAS signal and background noise as a function of QCL average output power at amplitude modulation mode. (b) Signal-to-noise ratio as a function of QCL output power. Data were obtained with a 500 ppb DMMP/zero air mixture.

evaluation tests were performed at an optimum excitation power of 65.5 mW, corresponding to the driving current of 645 mA, to determine the minimum detection limit.

For the QEPAS technique, the photoacoustic signal is pressure-dependent, since the pressure can affect the vibrational-translational (V-T) relaxation rate of the target gas, the absorption cross-section of absorbing molecules, and the number density N of the target gas molecules. On the other hand, both the resonant frequency and quality factor of the QTF also depend on the gas pressure, affecting the laser modulation frequency. Therefore, to obtain the maximum QEPAS signal, both the gas pressure and the laser modulation frequency must be optimized. The normalized signal for the 500 ppbv DMMP/zero air mixture at room temperature of 25 ℃ as a function of laser modulation frequency is shown in Fig. 5 for the various pressures. It was found that the relationship between the QEPAS signal and the modulation frequency exhibited a Lorentzian shape, while the optimum modulation frequency increased when the pressure decreased. Although the *Q*-factor of the QTF decreases with increasing pressure, collisions between molecules occur more frequently at higher pressure, and thus the V-T relaxation rate becomes fast. The combined action of these factors results in the maximum photoacoustic signal being observed at 700 Torr.

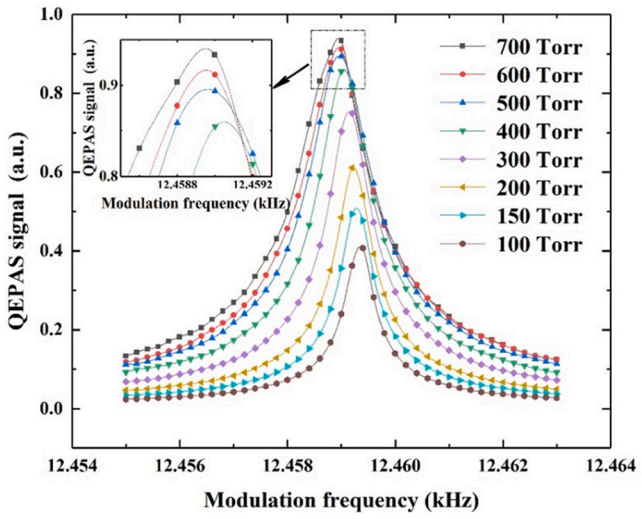

Fig. 5. Relationship between the normalized signal of a 500 ppb DMMP/zero air mixture and the laser modulation frequency for the different pressures from 100 Torr to 700 Torr.

Hence, the atmospheric pressure was selected as the operating pressure of the sensor, and the laser modulation frequency was set to 12.459 kHz.

3. Assessment of the sensor performance

Using the optimal operating parameters, including the laser power, the modulation frequency, and the gas pressure, we evaluated the performance of the DMMP sensor in terms of linearity, detection sensitivity, Allan-Werle deviation analysis, and selectivity verification. The results for stepwise DMMP concentration measurements from 0.2 ppm to 1.5 ppm are shown in Fig. 6. The QEPAS signal for each concentration step was measured for > 5 min, and the acquisition speed was 400 ms per point. After each DMMP concentration changed, we stopped the signal acquisition for 13 min to obtain a stable gas concentration. The average values of the results for each step as a function of the DMMP concentrations are plotted in Fig. 6(b). The linear fit yields a slope of 0.67 μV/ppb with an intercept of 355 μV, in agreement with the 380-μV background noise level measured in zero air. The calculated *R*-squared value is equal to 0.998, which confirms the linearity of the sensor system's response to DMMP concentration levels. When a 200-ppb DMMP/zero air mixture was flushed into the system, the SNR was 33.3, resulting in a 6-ppb minimum detection limit.

An Allan-Werle deviation analysis was performed, predicting the trend of the 1σ noise fluctuations as a function of the integration time at room temperature and atmosphere pressure. Based on the Allan deviation plot shown in Fig. 7, the 1σ noise can be reduced by further averaging the signal over a longer time, and a minimum detection limit of 0.45 ppb was achieved at the integration time of 20 s. For a longer integration time, the system drift is dominant due to the drift of the laser wavelength and the mechanical vibration of the vacuum pump. The stability of the sensing system can be further improved by using a frequency-locked system and a low-vibration pump.

4. DMMP measurement in real environments

For DMMP detection in a real environment, the QEPAS-based DMMP sensor must have high selectivity to avoid false alarms. The selectivity of the sensor was evaluated in two different measurement scenarios: (1) 500 ppb DMMP/zero air mixture and zero air were alternately fed into the gas chamber to obtain a standard reference signal. (2) 500 ppb DMMP/outdoor air and outdoor air were alternately fed into the gas chamber to obtain an actual signal in outdoor air. The main difference between the two tests is that the relative humidity of 47.2 % in outdoor air is higher than that of 0.011 % in zero air. The results of these two tests are plotted in Fig. 8. It was observed that the time needed for stable

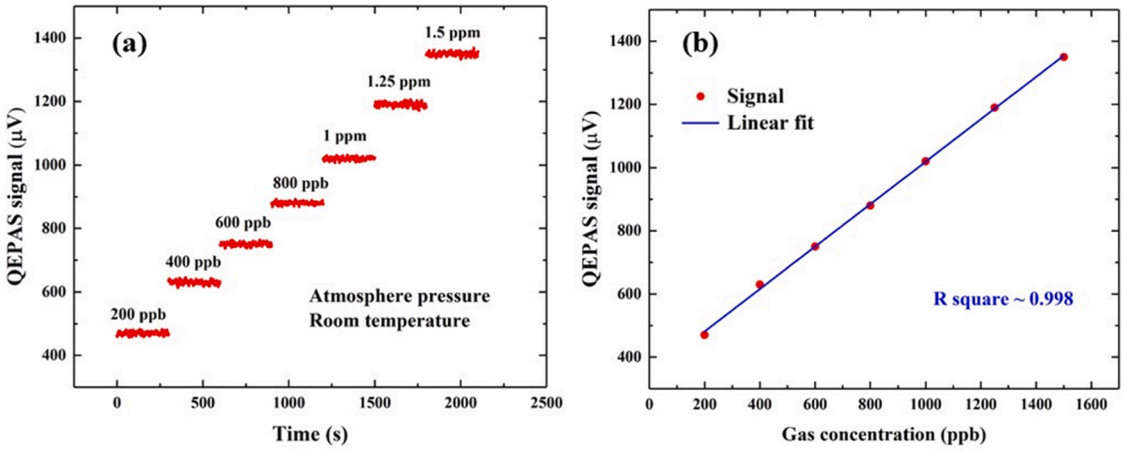

Fig. 6. (a) QEPAS signals recorded as a function of time at different DMMP concentration levels. (b) Same data averaged and plotted as a function of the DMMP concentration.

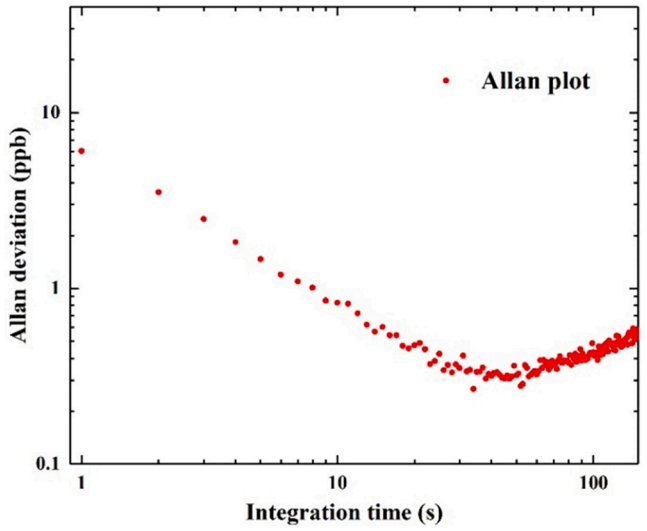

Fig. 7. Allan deviation analysis from time series measurements in zero air for the QEPAS-based DMMP sensor system.

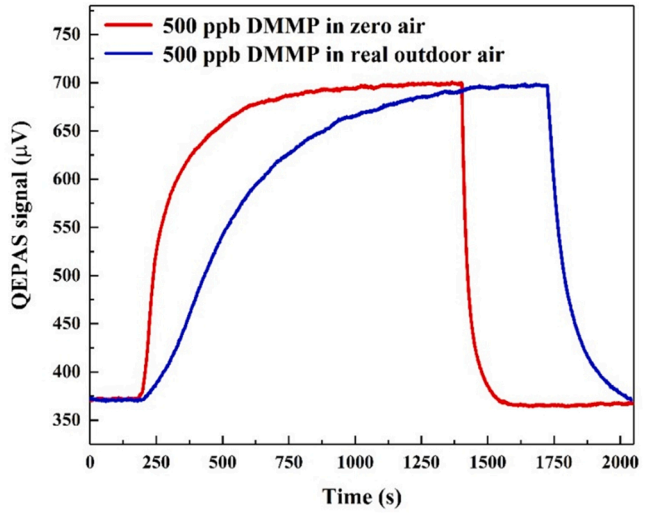

Fig. 8. Continuous photoacoustic signals recorded in two different measurement scenarios.

photoacoustic signal values was different for the two tests, which is because the influence of humidity in the environment increased the adsorption effect of DMMP on the air chamber wall and pipeline, and thus a longer stabilization time was needed in a real environment. However, the same final signal amplitude confirms the high selectivity of the DMMP detection in actual outdoor air.

5. Conclusions

The QEPAS-based sensor has high versatility due to its wavelength independence, which makes it possible to detect various nerve agents by replacing the laser sources. In this work, a ppb-level QEPAS-based DMMP sensor was developed with a compact size and reliable performance for the first time. An excitation wavelength of 9.56 μm was chosen for the strongest DMMP band which is interference-free from H_2O and CO_2. The main system parameters, including the laser excitation power, the gas pressure, and the modulation frequency, were optimized. Finally, the sensor linearity was verified in the range of 0 – 1.5 ppm and a minimum detection limit of 6 ppb at an integration time of 300 ms was achieved. We detected 500 ppb DMMP with real outdoor air as the carrier gas and obtained the same signal amplitude as that with zero air as the carrier gas, which verified the high selectivity of the sensor. The developed sensor paves the way for monitoring nerve agents in public places like airports, railroad stations, sports arenas, and ports. In the future, time division multiplexing technology can be introduced to couple multiple continuously tunable lasers with different center wavelengths into a sensor system, which would provide a broad wavelength detecting range, allowing for the simultaneous detection of several nerve agents of interest. Open gas chamber design and replacement of the current QCL driver with new electronics promise further to reduce the total sensor volume.

Declaration of Competing Interest

The authors declare that they have no known competing financial interests or personal relationships that could have appeared to influence the work reported in this paper.

Data availability

Data will be made available on request.

Acknowledgements

This work was supported by National Key R&D Program of China

(No. 2019YFE0118200); National Natural Science Foundation of China (NSFC) (Nos. 62235010 , 62175137, 62122045, 62075119); The Shanxi Science Fund for Distinguished Young Scholars (20210302121003); THORLABS GmbH, within PolySense, a joint-research laboratory.

References

[1] F. Arduini, A. Aziz, D. Moscone, F. Ricci, G. Palleschi, Fast, sensitive and cost-effective detection of nerve agents in the gas phase using a portable instrument and an electrochemical biosensor, Anal. Bioanal. Chem. 388 (5) (2007) 1049–1057.
[2] F. Di Pietrantonio, M. Benetti, D. Cannatà, E. Verona, A. Palla-Papavlu, V. Dinca, M. Dinescu, T. Mattle, T. Lippert, Volatile toxic compound detection by surface acoustic wave sensor array coated with chemoselective polymers deposited by laser induced forward transfer: application to sarin, Sens. Actuators B Chem. 174 (2012) 158–167.
[3] E. Brunol, F. Berger, M. Fromm, R. Planade, Detection of dimethyl methylphosphonate (DMMP) by tin dioxide-based gas sensor: response curve and understanding of the reactional mechanism, Sens. Actuators B Chem. 120 (1) (2006) 35–41.
[4] E.L. Holthoff, D.A. Heaps, P.M. Pellegrino, Development of a MEMS-scale photoacoustic chemical sensor using a quantum cascade laser, IEEE Sens. J. 10 (3) (2010) 572–577.
[5] C.A. Sanders, M. Rodriguez Jr, E. Greenbaum, Stand-off tissue-based biosensors for the detection of chemical warfare agents using photosynthetic fluorescence induction, Biosens. Bioelectron. 16 (7–8) (2001) 439–446.
[6] C. Olguín, N. Laguarda-Miro, L. Pascual, E. García-Breijo, R. Martinez-Manez, J. Soto, An electronic nose for the detection of Sarin, Soman and Tabun mimics and interfering agents, Sens. Actuators B Chem. 202 (2014) 31–37.
[7] J.F. Schneider, A.S. Boparai, L.L. Reed, Screening for Sarin in air and water by solid-phase microextraction–gas chromatography–mass spectrometry, J. Chromatogr. Sci. 39 (10) (2001) 420–424.
[8] M. Pohanka, J.Z. Karasova, K. Kuca, J. Pikula, O. Holas, J. Korabecny, J. Cabal, Colorimetric dipstick for assay of organophosphate pesticides and nerve agents represented by paraoxon, sarin and VX, Talanta 81 (1–2) (2010) 621–624.
[9] P. Wang, J. Yu, Z. Li, Z. Ding, L. Guo, B. Du, Synthesis and evaluation of a new phthalocyanine as sensor material for sarin detection, Sens. Actuators B Chem. 188 (2013) 1306–1311.
[10] Y. Zhao, J. He, M. Yang, S. Gao, G. Zuo, C. Yan, Z. Cheng, Single crystal WO_3 nanoflakes as quartz crystal microbalance sensing layer for ultrafast detection of trace sarin simulant, Anal. Chim. Acta 654 (2) (2009) 120–126.
[11] L.A. Patil, A.R. Bari, M.D. Shinde, V. Deo, M.P. Kaushik, Detection of dimethyl methyl phosphonate – a simulant of sarin: the highly toxic chemical warfare – using platinum activated nanocrystalline ZnO thick films, Sens. Actuators B Chem. 161 (1) (2012) 372–380.
[12] M.E. Webber, M. Pushkarsky, C. Kumar, N. Patel, Fiber-amplifier-enhanced photoacoustic spectroscopy with near-infrared tunable diode lasers, Appl. Opt. 42 (12) (2003) 2119–2126.
[13] X. Yin, L. Dong, H. Wu, H. Zheng, W. Ma, L. Zhang, W. Yin, S. Jia, F.K. Tittel, Sub-ppb nitrogen dioxide detection with a large linear dynamic range by use of a differential photoacoustic cell and a 3.5 W blue multimode diode laser, Sens. Actuators B Chem. 247 (2017) 329–335.
[14] A. Elia, P.M. Lugarà, C. Di Franco, V. Spagnolo, Photoacoustic techniques for trace gas sensing based on semiconductor laser sources, Sensors 9 (12) (2009) 9616–9628.
[15] Y. Pan, L. Dong, X. Yin, H. Wu, Compact and highly sensitive NO_2 photoacoustic sensor for environmental monitoring, Molecules 25 (5) (2020) 1201.
[16] K. Chen, H. Deng, M. Guo, C. Luo, S. Liu, B. Zhang, F. Ma, F. Zhu, Z. Gong, W. Peng, Q. Yu, Tube-cantilever double resonance enhanced fiber-optic photoacoustic spectrometer, Opt. Laser Technol. 123 (2020), 105894.
[17] J. Luo, Y.H. Fang, Y.D. Zhao, A.J. Wang, D.C. Li, Y.Y. Li, Y. Liu, F.X. Cui, J. Wu, J. X. Liu, Research on the detection of SF_6 decomposition products based on nonresonant photoacoustic spectroscopy, Anal. Methods 7 (3) (2015) 1200–1207.
[18] A.A. Kosterev, Y.A. Bakhirkin, R.F. Curl, F.K. Tittel, Quartz-enhanced photoacoustic spectroscopy, Opt. Lett. 27 (21) (2002) 1902–1904.
[19] P. Patimisco, A. Sampaolo, L. Dong, F.K. Tittel, V. Spagnolo, Recent advances in quartz enhanced photoacoustic sensing, Appl. Phys. Rev. 5 (1) (2018), 011106.
[20] L. Dong, H. Wu, H. Zheng, Y. Liu, X. Liu, W. Jiang, L. Zhang, W. Ma, W. Ren, W. Yin, S. Jia, F.K. Tittel, Double acoustic microresonator quartz-enhanced photoacoustic spectroscopy, Opt. Lett. 39 (8) (2014) 2479–2482.
[21] F. Wang, J. Chang, Q. Wang, Y. Liu, Z. Liu, Z. Qin, C. Zhu, Improvement in QEPAS system based on miniaturized collimator and flat mirror, Opt. Commun. 381 (2016) 152–157.
[22] H. Wu, L. Dong, H. Zheng, Y. Yu, W. Ma, L. Zhang, W. Yin, L. Xiao, S. Jia, F. K. Tittel, Beat frequency quartz-enhanced photoacoustic spectroscopy for fast and calibration-free continuous trace-gas monitoring, Nat. Commun. 8 (1) (2017) 1–8.
[23] K. Liu, X. Guo, H. Yi, W. Chen, W. Zhang, X. Gao, Off-beam quartz-enhanced photoacoustic spectroscopy, Opt. Lett. 34 (10) (2009) 1594–1596.
[24] L. Dong, A.A. Kosterev, D. Thomazy, F.K. Tittel, QEPAS spectrophones: design, optimization, and performance, Appl. Phys. B 100 (3) (2010) 627–635.
[25] W. Ren, W.Z. Jiang, F.K. Tittel, Single-QCL-based absorption sensor for simultaneous trace-gas detection of CH_4 and N_2O, Appl. Phys. B 117 (1) (2014) 245–251.
[26] Z. Shang, H. Wu, S. Li, F.K. Tittel, L. Dong, Elliptical-tube off-beam quartz-enhanced photoacoustic spectroscopy, Appl. Phys. Lett. 120 (17) (2022), 171101.
[27] N. Maurin, R. Rousseau, W. Trzpil, G. Aoust, M. Hayot, J. Mercier, M. Bahriz, F. Gouzi, A. Vicet, First clinical evaluation of a quartz enhanced photo-acoustic CO sensor for human breath analysis, Sens. Actuators B Chem. 319 (2020), 128247.
[28] Y. Ma, Y. Hong, S. Qiao, Z. Lang, X. Liu, H-shaped acoustic micro-resonator-based quartz enhanced photoacoustic spectroscopy, Opt. Lett. 47 (3) (2022) 601–604.
[29] T. Wei, A. Zifarelli, S.D. Russo, H. Wu, G. Menduni, P. Patimisco, A. Sampaolo, V. Spagnolo, L. Dong, High and flat spectral responsivity of quartz tuning fork used as infrared photodetector in tunable diode laser spectroscopy, Appl. Phys. Rev. 8 (4) (2021), 041409.
[30] Y. Cao, R. Wang, J. Peng, K. Liu, W. Chen, G. Wang, X. Gao, Humidity enhanced N_2O photoacoustic sensor with a 4.53 μm quantum cascade laser and Kalman filter, Photoacoustics 24 (2021), 100303.
[31] Y. He, Y. Ma, Y. Tong, X. Yu, Z. Peng, J. Gao, F.K. Tittel, Long distance, distributed gas sensing based on micro-nano fiber evanescent wave quartz-enhanced photoacoustic spectroscopy, Appl. Phys. Lett. 111 (2017), 241102.
[32] H. Wu, A. Sampaolo, L. Dong, P. Patimisco, X. Liu, H. Zheng, X. Yin, W. Ma, L. Zhang, W. Yin, V. Spagnolo, S. Jia, F.K. Tittel, Quartz enhanced photoacoustic H_2S gas sensor based on a fiber-amplifier source and a custom tuning fork with large prong spacing, Appl. Phys. Lett. 107 (2015), 111104.
[33] A. Sampaolo, P. Patimisco, M. Giglio, A. Zifarelli, H. Wu, L. Dong, V. Spagnolo, Quartz-enhanced photoacoustic spectroscopy for multi-gas detection: a review, Anal. Chim. Acta 1202 (2021), 338894.
[34] M. Giglio, A. Elefante, P. Patimisco, A. Sampaolo, F. Sgobba, H. Rossmadl, V. Mackowiak, H. Wu, F.K. Tittel, L. Dong, V. Spagnolo, Quartz-enhanced photoacoustic sensor for ethylene detection implementing optimized custom tuning fork-based spectrophone, Opt. Express 27 (4) (2019) 4271–4280.
[35] S. Li, L. Dong, H. Wu, A. Sampaolo, P. Patimisco, V. Spagnolo, F.K. Tittel, Ppb level quartz-enhanced photoacoustic detection of carbon monoxide exploiting a surface grooved tuning fork, Anal. Chem. 91 (9) (2019) 5834–5840.
[36] P. Patimisco, A. Sampaolo, L. Dong, M. Giglio, G. Scamarcio, F.K. Tittel, V. Spagnolo, Analysis of the electro-elastic properties of custom quartz tuning forks for optoacoustic gas sensing, Sens. Actuators B Chem. 227 (2016) 539–546.
[37] Z. Shang, S. Li, B. Li, H. Wu, A. Sampaolo, P. Patimisco, V. Spagnolo, L. Dong, Quartz-enhanced photoacoustic NH_3 sensor exploiting a large-prong-spacing quartz tuning fork and an optical fiber amplifier for biomedical applications, Photoacoustics 26 (2022), 100363.
[38] C. Zhang, S. Qiao, Y. Ma, Highly sensitive photoacoustic acetylene detection based on differential photoacoustic cell with retro-reflection-cavity, Photoacoustics 30 (2023), 100467.
[39] S. Qiao, P. Ma, V. Tsepelin, G. Han, J. Liang, W. Ren, H. Zheng, Y. Ma, Super tiny quartz-tuning-fork-based light-induced thermoelastic spectroscopy sensing, Opt. Lett. 2 (48) (2023) 419–422.
[40] X. Liu, S. Qiao, G. Han, J. Liang, Y. Ma, Highly sensitive HF detection based on absorption enhanced light-induced thermoelastic spectroscopy with a quartz tuning fork of receive and shallow neural network fitting, Photoacoustics 28 (2022), 100422.
[41] X. Yin, Lei Dong, H. Wu, M. Gao, L. Zhang, X. Zhang, L. Liu, X. Shao, F.K. Tittel, Compact QEPAS humidity sensor in SF_6 buffer gas for high-voltage gas power systems, Photoacoustics 25 (2022), 100319.

Zhijin Shang is now pursuing a Ph.D. degree in atomic and molecular physics in the Institute of Laser Spectroscopy of Shanxi university, China. His research interests include optical sensors and photoacoustic spectroscopy.

Hongpeng Wu received his Ph.D. degree in atomic and molecular physics from Shanxi niversity, China, in 2017. From 2015–2016, he studied as a joint Ph.D. student in the electrical and computer engineering department and rice quantum institute, Rice University, Houston, USA. Currently he is a professor in the Institute of Laser Spectroscopy of Shanxi University. His research interests include optical sensors and laser spectroscopy techniques.

Shangzhi Li received his Ph.D. degree in atomic and molecular physics from Shanxi niversity, China, in 2022. His research interests include gas sensor and spectroscopic techniques for real-time monitoring.

Gang Wang is now pursuing a Ph.D. degree in atomic and molecular physics in the Institute of Laser Spectroscopy of Shanxi university, China. His research interests include optical sensors and laser spectroscopy techniques.

Angelo Sampaolo obtained his Master degree in Physics in 2013 and the Ph.D. Degree in Physics in 2017 from University of Bari. He was an associate researcher in the Laser Science Group at Rice University from 2014 to 2016 and associate researcher at Shanxi University since 2018. Since May 2017, he was a Post-Doctoral Research associate at University of Bari and starting from December 2019, he is Assistant Professor at Polytechnic of Bari. His research activity has included the study of the thermal properties of heterostructured devices via Raman spectroscopy. Most recently, his research interest has focused on the development of innovative techniques in trace gas sensing, based on Quartz-Enhanced Photoacoustic Spectroscopy and covering the full spectral range from near-IR to THz. His achieved results have been acknowledged by a cover paper in Applied Physics Letter of the July 2013 issue.

Pietro Patimisco obtained the Master degree in Physics (cum laude) in 2009 and the Ph.D. Degree in Physics in 2013 from the University of Bari. Since 2018, he is Assistant professor at the Technical University of Bari. He was a visiting scientist in the Laser Science Group at Rice University in 2013 and 2014. Dr. Patimisco's scientific activity addressed both micro-probe optical characterization of semiconductor optoelectronic devices and optoacoustic gas sensors. Recently, his research activities included the study and applications of trace-gas sensors, such as quartz-enhanced photoacoustic spectroscopy and cavity enhanced absorption spectroscopy in the mid infrared and terahertz spectral region, leading to several publications, including a cover paper in Applied Physics Letter of the July 2013 issue.

Vincenzo Spagnolo obtained the Ph.D. in physics in 1994 from University of Bari. From 1997–1999, he was researcher of the National Institute of the Physics of Matter. Since 2004, he works at the Technical University of Bari, formerly as assistant and associate professor and, starting from 2018, as full Professor of Physics. Since 2019, he is vice-rector of the Technical University of Bari, deputy to technology transfer. He is the director of the joint-research lab PolySense between Technical University of Bari and THORLABS GmbH, fellow member of SPIE and senior member of OSA. His research interests include opto-acoustic gas sensing and spectroscopic techniques for real-time monitoring. His research activity is documented by more than 220 publications and two filed patents. He has given more than 50 invited presentations at international conferences and workshops.

Lei Dong received his Ph.D. degree in optics from Shanxi University, China, in 2007. From June, 2008 to December, 2011, he worked as a post-doctoral fellow in the Electrical and Computer Engineering Department and Rice Quantum Institute, Rice University, Houston, USA. Currently he is a professor in the Institute of Laser Spectroscopy of Shanxi University. His research activities research activities are focused on research and development in laser spectroscopy, in particular photoacoustic spectroscopy applied to sensitive, selective and real-time trace gas detection, and laser applications in environmental monitoring, chemical analysis, industrial process control, and medical diagnostics. He has published more than 100 peer reviewed papers with $>$ 2200 positive citations.